Dynamics characteristics of a rotor-casing system subjected to axial load and radial rub

Yang Yang, Yuqian Xu, Yiren Yang, Dengqing Cao

Dynamics characteristics of a rotor-casing system subjected to axial load and radial rub

Yang Yang[1*], Yuqian Xu[2], Yiren Yang[1], Dengqing Cao[2]

1. School of Mechanics and Engineering, Southwest Jiaotong University, Chengdu 610031, China

2. School of Astronautics, Harbin Institute of Technology, PO Box 137, Harbin 150001, China

Abstract: Aiming at the coupling fault of axial load and radial rub, a geometric nonlinear rotor-casing system is developed in this paper. For the actual case that the aero-engine components (i.e. compressor disc, turbine disc, stator casing, combustor and so on) are sprayed with thermal barrier coatings, the interaction between disc and casing is refined into four stages, including no rub, low rub, rub and high rub. With the increase of invasion depth, the corresponding force models are applied to describe the different impact mechanism. The frictional characteristic between disc and casing is described by the Coulomb model. Then the linear interpolation is used to predict the instantaneous contact of disc-casing and the nonlinear dynamic behaviors of the rotor-casing system subjected to axial load and radial rub are analyzed in the form of bifurcation diagram. Moreover, the rub-impact forms, such as full annular rubbing and partial rubbing, are identified by whirl orbit and waveform. On this basis, the dynamic comparison of the rotor system with/without axial load is conducted. The response variations caused by coating hardness and support stiffness of casing are further discussed.

Key words: rotor-casing system, axial load, radial rub, nonlinear dynamic behavior

1. Introduction

In recent years, larger axial load acting on rotors becomes a big issue regarding reliability of compressor, especially for applications in high temperature heat pump system [1-3]. Due to atmospheric turbulence, non-uniform combustion, installation preload and so on, rotating machine is often subjected to axial load, which may affect natural whirl speed, vibration stability and nonlinear dynamic behaviors [4].

Generally speaking, axial load acting on the rotating machine can be classified as constant force, periodic force and random force. Under this circumstance, a large number of researchers have

*Corresponding author: Yang Yang, 181042yy@163.com; Yuqian Xu, xuyuqianscience@126.com; Yiren Yang, yangyiren05@126.com; Dengqing Cao, dqcao@hit.edu.cn

focused on the dynamic characteristics of rotating machine with effect of axial load. Aiming at a constant axial force, Nelson [5] established a rotating shaft model and then analyzed the natural characteristics, including critical speed and vibration mode. Chen et al. [6] analyzed the dynamic behavior of a rotating composite shaft subjected to periodic axial load. Meanwhile, the effects of rotational speed and disc eccentricity on the unstable regions of the system were investigated in [6]. Additionally, Leng et al. [7] studied the bifurcation characteristics of a cracked rotor system with random axial load and obtained the variation routes going in and out of chaotic region. By using the Lagrange equations, Chen et al. [8] obtained the nonlinear stability of the rotating shaft-disc system with sliding supported condition and periodic axial load. As can be seen, axial load plays an increasingly important role in stability and dynamic characteristic of rotating machine and should be paid enough attention in the strength design.

Radial rub-impact between rotor and stator is another important factor, which directly affects the well operation of rotating machine. In order to pursue higher efficiency and larger thrust weight ratio, smaller initial clearance of rotor-stator is widely accepted in the structural design [9-12]. Therefore, the possibility of rub-impact fault increases dramatically. The physical impact of the rotor on the stationary elements of a rotating machine and the subsequent rubbing at the contact area cause a serious malfunction that may lead to catastrophic failure [13]. To predict dynamic characteristic of rotor system with rub-impact fault, numerous articles on this topic have been published. Taking a Jeffcott rotor with a given initial clearance and cross-coupling influences as the research object, Jiang and Ulbrich [14] studied the stability of the full annular rub solutions. Yu [15] studied the influences of disc eccentricity, initial clearance, frictional coefficient and structural damping on the full annular rubbing. Chu et al. [16] investigated the periodic, quasi-periodic and chaotic motion of a Jeffcott rotor system with imbalance-rub coupling fault. Vlajic et al. [17] analytically and numerically investigated torsional vibration of an unbalanced Jeffcott rotor subjected to continuous stator contact. By using the laboratory scale drilling apparatus, they further tested torsional vibration of a rotor enclosed within a stator subjected to dry friction [18]. To identify rub-impact characteristic of cracked rotor, Patel and Darpe [19] analyzed the directional nature of the higher harmonics and found the nature of $2X$ and higher harmonics at the sub harmonic resonances. When dealing with the partial rub of the generator, Huang et al. [20] explored the nonlinear behaviors of the rotor system with imbalance and parallel misalignment. Xiang et al. [21] proposed an asymmetric double-disc

rotor-bearing system and then analyzed the interaction between rub-impact force and oil-film force.

Characterization of rub-impact mechanism is the crucial basis of predicting the dynamic characteristics of the rotor system with rub-impact. As mentioned in [22,23], when the aero-engine components are sprayed with coatings [24,25], both local deformation of coatings and structural deformation of components coexist during the rub-impact process. However, existing publications about coatings mainly focus on the material characteristics of coatings or static behaviors of aero-engine components with coatings [26,27]. Therefore, dynamic investigation of rotor-stator system with coatings should be given rise to a widely attention.

So far single fault effect of axial load or radial rub has been investigated in detail. However, considering the application of surface coatings, pioneering contributions to dynamic variation of rotor system with coupling influence of axial load-radial rub have not been observed in existing literature. Actually, it is of practical significance for the purpose of guaranteeing run quality. In the authors' previous work [28], a geometric nonlinear rotor system without axial load and casing has been established and the single rub-impact fault has been analyzed. On this basis, a more complicated dynamic model of rotor-casing system subjected to axial load and radial rub is further proposed in this paper. According to the penetration of disc-casing, the rub-impact process is divided into four stages, including no rub, low rub, rub and high rub. The tangential frictional force of disc-casing is described by the Coulomb model [29]. Then, the nonlinear dynamic characteristics of the rotor system are analyzed by bifurcation diagram. Particularly, the relation between axial load and radial rub is identified by using whirl orbit and waveform. Moreover, the dynamic variations caused by coating hardness and support stiffness of casing are revealed, such as rub-impact degree, rub-impact form and rotational speed of first rub-impact.

2. Mathematical formulation

During rotor operation, there are three main vibration modes – lateral, torsional and axial modes. Generally, the effect of torsional vibration is weaker than that of lateral vibration. Therefore, the whirling motion of rotor is of the greatest concern in the actual rotating machine.

Take a rotor-casing system subjected to axial load as the research object. As shown in Fig. 1, the rigid disc with eccentricity is mounted on the elastic shaft, which is subjected to constant axial load. The casing is supported by the linear springs and viscous dampers. During the whirling motion with

larger amplitude, the geometric relationship of strain-displacement becomes nonlinear and the material relationship of stress-strain is assumed to be linear. According to the actual case of aero-engine, the disc and the casing are sprayed with thermal barrier coatings.

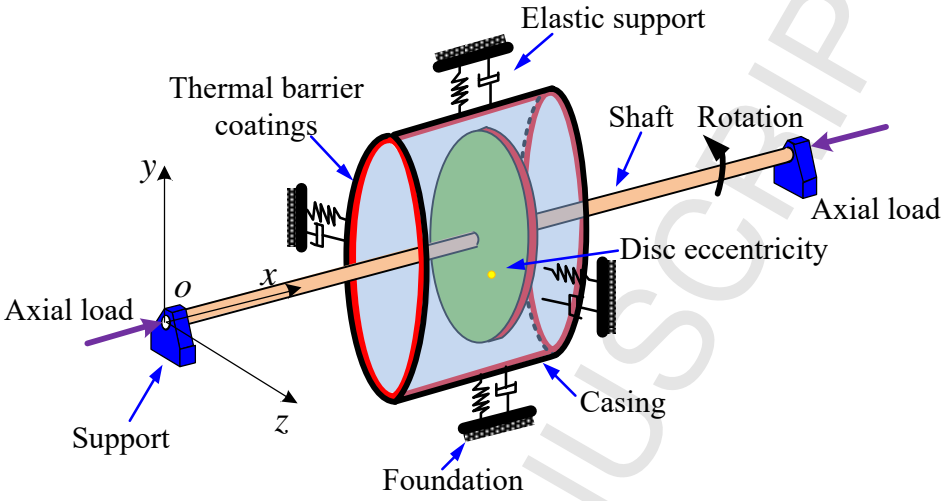

Fig. 1. Schematic diagram of a rotor-casing system subjected to axial load.

In order to analyze the vibration characteristics of the rotor-casing system, some assumptions are made during the process of dynamic modeling, including

(1) The origin of the global coordinate system ($o-xyz$) locates at the left end of shaft and the axis $o-x$ coincides with the elastic axis of shaft.

(2) Compared with transverse deformation, the axial deformation of shaft is much smaller and then ignored.

(3) The mass of shaft is far less than that of disc and not taken into consideration.

(4) The thermal effect and friction torque are ignored during the rub-impact process of disc-casing.

2.1 Dynamic modeling of shaft subjected to axial load

In this section, the dynamic modeling of the shaft subjected to axial load is established. The flexible shaft is described by the simply-supported Euler-Bernoulli beam subjected to the constant axial load N. Meanwhile, in the plane xoy, the interactional force between disc and shaft is expressed as F_a.

Due to the constant axial load, the initial strain of the flexible shaft can be expressed as

$$\varepsilon_0 = -\frac{N}{EA} \tag{1}$$

where E denotes the elastic modulus of shaft, A denotes the area of cross section of shaft.

Fig. 2 shows the deformation diagram of micro segment with the effect of axial load, where $i_{\xi 1} - o_1 - i_{\eta 1}$ and $i_{\xi 2} - o_2 - i_{\eta 2}$ are the local coordinate systems at both sides of micro segment, respectively. β denotes the angle relationship between two local coordinate systems. η denotes the distance between arbitrary point A and center of cross section O_1 in the local coordinate system $i_{\xi 1} - o_1 - i_{\eta 1}$.

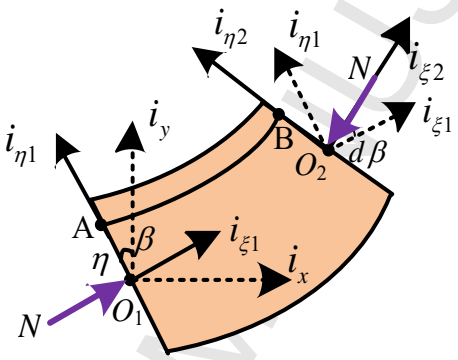

Fig. 2. Schematic diagram of micro segment deformation with effect of axial load.

Due to the large unbalanced force of disc, the phenomenon of whirling motion with large amplitude occurs, which leads to the obvious geometric nonlinearity of shaft. In this case, the transverse bending strain of shaft without axial load has been derived in [28], namely

$$\varepsilon_{11}^{*} = \varepsilon - \eta\beta' \tag{2}$$

where the elongation of the elastic axis ε and the first partial derivate of angle β' respectively obey

$$\begin{cases} \varepsilon = \sqrt{1+(w')^2} - 1 \\ \beta' = \dfrac{w''}{1+(w')^2} \end{cases} \tag{3}$$

where w denotes the transverse deformation.

According to Eqs. (1) and (2), the total transverse strain of the Euler-Bernoulli beam subjected to axial load can be written as

$$\varepsilon_{11}=\varepsilon_0+\sqrt{1+\left(w'\right)^2}-1-\beta'\eta \tag{4}$$

The above expression suggests that the total strain is composed of the initial strain and the bending strain.

Let us define the potential energy unit length as V_{unit} and then the first variation of V_{unit} can be expressed as

$$\begin{aligned}\delta V_{\text{unit}} &= \iint E\varepsilon_{11}\delta\varepsilon_{11}dA \\ &=\iint E\left(\varepsilon_0+\sqrt{1+\left(w'\right)^2}-1-\beta'\eta\right)\delta\left(\varepsilon_0+\sqrt{1+\left(w'\right)^2}-1-\beta'\eta\right)dA \\ &=\iint E\left(\varepsilon_0+\sqrt{1+\left(w'\right)^2}-1-\beta'\eta\right)dA\frac{w'}{\sqrt{1+\left(w'\right)^2}}\delta w' \\ &-\iint E\left(\varepsilon_0+\sqrt{1+\left(w'\right)^2}-1-\beta'\eta\right)\eta dA\delta\beta'\end{aligned} \tag{5}$$

where the first variation of the initial potential energy generated by the initial strain ε_0 can be expressed as

$$\delta V_0=\iint E\varepsilon_0 dA\frac{w'}{\sqrt{1+\left(w'\right)^2}}\delta w'-\iint E\varepsilon_0\eta dA\delta\beta' \tag{6}$$

Since that the cross section of the shaft shown in Fig. 1 is circular, the static moment and the inertia moment of area can satisfy

$$\iint \eta dA=0\ ,\ \iint \eta^2 dA=I \tag{7}$$

Therefore, the first variation of the initial potential energy is further simplified as

$$\begin{aligned}\delta V_0&=\iint E\varepsilon_0 dA\frac{w'}{\sqrt{1+\left(w'\right)^2}}\delta w' \\ &=-N\frac{w'}{\sqrt{1+\left(w'\right)^2}}\delta w'\end{aligned} \tag{8}$$

By using the Taylor series expansion, Eq. (8) can be expressed in the form of three orders, so that

$$\delta V_0=-N\left(w'-\frac{\left(w'\right)^3}{2}\right)\delta w' \tag{9}$$

Due to the assumption (3) that the mass of the shaft is ignored, the first variation of the kinetic

energy unit length is $\delta T_{\text{unit}} = 0$. Thus, the Hamilton's principle of the whole Euler-Bernoulli beam can be expressed as

$$\int_{t_1}^{t_2} \left(\delta T - \delta V + \delta W_{nc} \right) dt = 0 \tag{10}$$

where the non-conservative work satisfies that

$$\int_{t_1}^{t_2} \delta W_{nc} dt = \int_{t_1}^{t_2} \int_0^l Q_{nc} \delta w dx dt \tag{11}$$

and the non-conservative force Q_{nc} contains the acting force of the disc and the damping force of shaft.

According to Eq. (10), the transverse vibration equation of the shaft in the plane xoy is given as

$$\left(EIw'' - 2EI\left(w'\right)^2 w'' \right)'' + \left(2EI\left(w''\right)^2 w' - \frac{1}{2} EA\left(w'\right)^3 \right)' + N\left(w' - \frac{\left(w'\right)^3}{2} \right)' = Q_{nc} \tag{12}$$

Due to the fact that the work rotational speed of actual aero-engine is in the range of the first order and second order critical speeds, the truncated modal number is set to $MN = 1$ during the discrete process of partial differential equation.

Meanwhile, the simply-supported condition of the flexible shaft can be expressed as

$$w\big|_{x=0} = 0, \;\; w''\big|_{x=0} = 0, \;\; w\big|_{x=l} = 0, \;\; w''\big|_{x=l} = 0 \tag{13}$$

Based on the above boundary condition, the characteristic function corresponding to the first order is supposed as

$$w = \delta_{l/2} \sin\left(\frac{\pi}{l} x \right), \;\; \dot{w} = \dot{\delta}_{l/2} \sin\left(\frac{\pi}{l} x \right) \tag{14}$$

where $\delta_{l/2}$ denotes the transverse displacement of the middle part in the shaft.

By substituting Eq. (14) into Eq. (12), the vibration equation of the shaft in the plane xoy can be written as

$$\left(EI\frac{\pi^4}{2l^3} - N\frac{\pi^2}{2l} \right)\delta_{l/2} + \left(EA\frac{3\pi^4}{16l^3} + N\frac{3\pi^4}{16l^3} \right)\delta_{l/2}^3 - EI\frac{\pi^6}{2l^5}\delta_{l/2}^3 + \frac{cl}{2}\dot{\delta}_{l/2} = F_a \tag{15}$$

Considering that the radius of shaft is much smaller than the length of shaft, the third term (i.e.

$EI\frac{\pi^6}{2l^5}$) in Eq. (15) can be ignored. Therefore, we can further define that

$$k_{eq}=EI\frac{\pi^4}{2l^3}-N\frac{\pi^2}{2l},\quad \alpha=EA\frac{3\pi^4}{16l^3}+N\frac{3\pi^4}{16l^3},\quad c_{eq}=\frac{cl}{2} \tag{16}$$

where k_{eq} denotes the equivalent linear stiffness of shaft, α denotes the equivalent nonlinear stiffness of shaft, and c_{eq} denotes the equivalent damping of shaft.

According to the definition shown in Eq. (16), Eq. (15) can be modified as

$$F_a=k_{eq}\delta_{l/2}+\alpha\delta_{l/2}^3+c_{eq}\dot{\delta}_{l/2} \tag{17}$$

Because of the circular cross section of shaft, the vibration equation of the shaft in the plane xoz keeps the same as that in the plane xoy. Therefore, an equivalent dynamic model of the rotor-casing system subjected to axial load is established, as shown in Fig. 3.

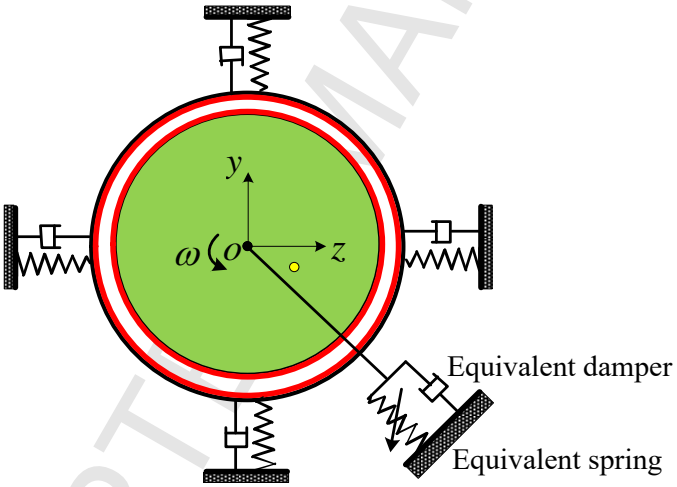

Fig. 3. Equivalent dynamic model of rotor-casing system with axial load.

After the above detailed derivations, the restoring force of the equivalent spring and equivalent damper depicted in Fig. 3 is written as

$$F=k_{eq}\delta_r+\alpha\delta_r^3+c_{eq}\dot{\delta}_r \tag{18}$$

where δ_r denotes the radial displacement of the disc, namely

$$\delta_r=\sqrt{z_1^2+y_1^2} \tag{19}$$

In Eq. (19), z_1 and y_1 denote the displacement components of the disc in the two directions, i.e. $o-z$ and $o-y$.

2.2 Rub-impact mechanism of disc-casing

Rub-impact fault of rotor-stator belongs to classical secondary fault that often occurs in rotating machine. When dealing with the rub-impact fault, the interaction between rotor and stator is usually identified as normal impact and tangential friction [30-34]. In other word, the collision direction is seen as perpendicular to the tangential direction of contact surface.

In this paper, the effects of the thermal barrier coatings painted on disc and casing are investigated, and the rub-impact mechanism of disc-casing with coatings is described by the novel force model that is recently proposed by the authors and examined on the rotor test rig [22,23]. The whole interaction process is divided into no rub, low rub, rub and high rub as shown in Fig. 4, where δ_0 denotes the initial clearance between rotor and stator, k_c denotes the structural stiffness of casing, k_h denotes the Hertz contact stiffness of surface coatings, χ is defined to describe the minor penetration and it is set to 1%.

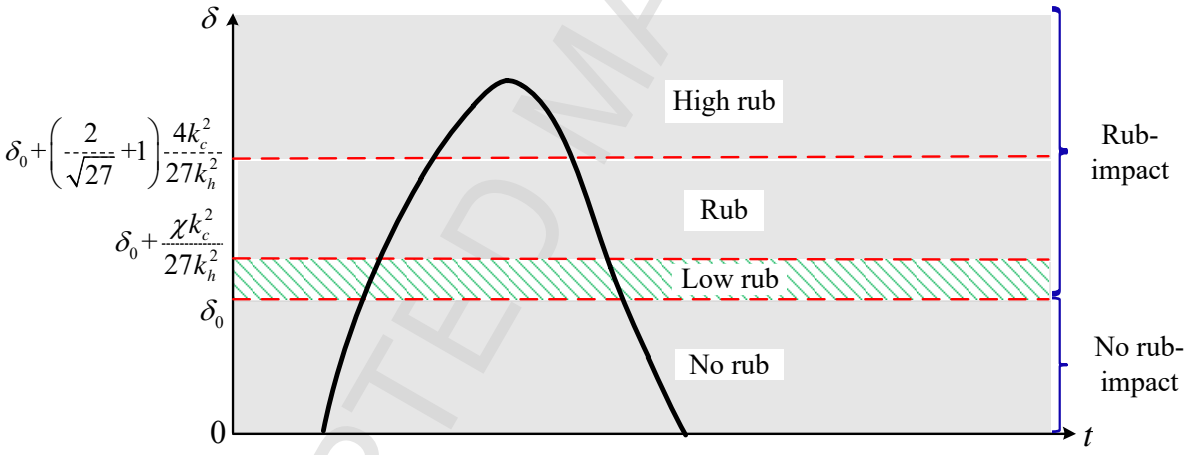

Fig. 4. Four rub-impact stages of disc-casing with thermal barrier coatings.

In the range $[0, \delta_0]$, there is no rub-impact fault between disc and casing. With the increase of penetration of disc-casing, in the range $\left[\delta_0, \delta_0+\frac{\chi k_c^2}{27k_h^2}\right]$, low rub happens and the total deformation is dominated by small coatings deformation. In the range $\left[\delta_0+\frac{\chi k_c^2}{27k_h^2}, \delta_0+\left(\frac{2}{\sqrt{27}}+1\right)\frac{\chi k_c^2}{27k_h^2}\right]$, rub happens and the total deformation consists of coatings deformation and small casing deformation. At last, when the condition $\delta \geq \delta_0+\left(\frac{2}{\sqrt{27}}+1\right)\frac{4k_c^2}{27k_h^2}$ is satisfied, the rub is identified as high one. At this

interval, the total deformation is composed of coatings deformation and casing deformation.

Therefore, the different impact force models in the above four stages are expressed as

$$F_N=\begin{cases}\dfrac{k_c k_h \delta_h^{\frac{1}{2}}}{k_c+k_h \delta_h^{\frac{1}{2}}}\left(\delta-\delta_0\right) & \delta \geq \delta_0+\left(\dfrac{2}{\sqrt{27}}+1\right)\dfrac{4k_c^2}{27k_h^2} \\ \dfrac{2\left(4^{3/2}-\chi^{3/2}\right)}{3\sqrt{27}\left(4-\chi\right)+2\left(4^{3/2}-\chi^{3/2}\right)}k_c\left(\delta-\delta_0\right) & \delta_0+\dfrac{\chi k_c^2}{27k_h^2} \leq \delta < \delta_0+\left(\dfrac{2}{\sqrt{27}}+1\right)\dfrac{4k_c^2}{27k_h^2} \\ \left(\dfrac{2\sqrt{27}}{\sqrt{\chi}}-\dfrac{54}{\chi}\ln\left(\sqrt{27}+\sqrt{\chi}\right)+\dfrac{54}{\chi}\ln\left(\sqrt{27}\right)\right)k_h\left(\delta-\delta_0\right)^{\frac{3}{2}} & \delta_0 \leq \delta < \delta_0+\dfrac{\chi k_c^2}{27k_h^2} \\ 0 & \delta < \delta_0\end{cases} \tag{20}$$

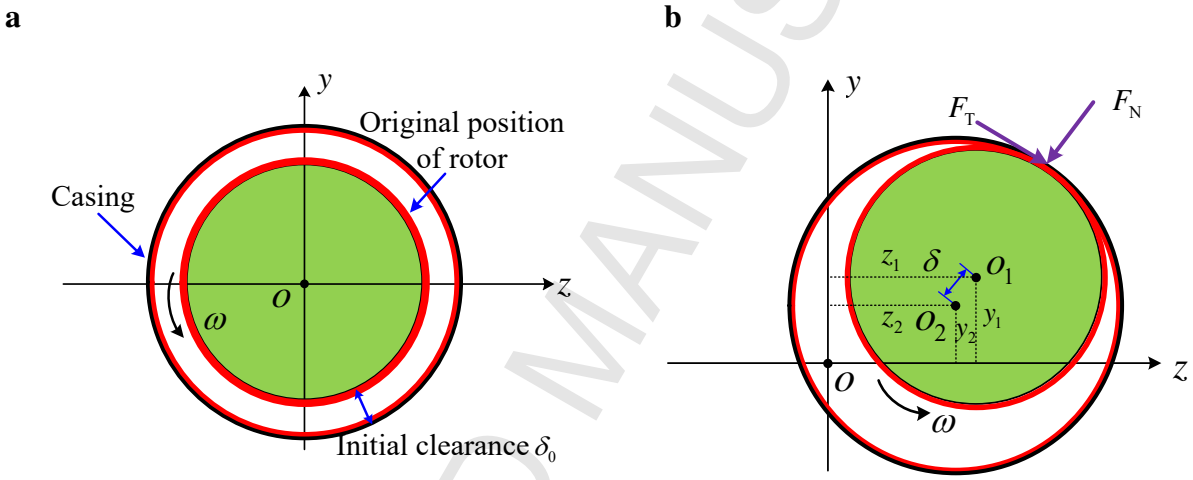

Fig. 5. Schematic diagram of rub-impact with surface coatings: (a) initial condition and (b) rub-impact condition.

As shown in Fig. 5, due to the fact that the casing is supported by the linear spring and the viscous damper, the rub penetration needs to be described by the relative motion between disc and casing, namely

$$\delta-\delta_0=\sqrt{\left(z_1-z_2\right)^2+\left(y_1-y_2\right)^2}-\delta_0=\delta_c+\delta_h \tag{21}$$

where z_2 and y_2 denote the displacement components of the casing in the two directions of $o-z$ and $o-y$. δ_c and δ_h denote the casing deformation and coatings deformation, respectively.

Referring to the authors' previous work, the inner relation between total deformation and coatings deformation obeys

$$\delta_h = \left(\frac{4^{1/3} f\left(\delta-\delta_0\right)}{6k_h} + \frac{k_c^2 4^{2/3}}{6k_h f\left(\delta-\delta_0\right)} - \frac{k_c}{3k_h} \right)^2 \tag{22}$$

where $f\left(\delta-\delta_0\right)$ is the function of the total penetration $\delta-\delta_0$, so that

$$f\left(\delta-\delta_0\right) = \left(k_c \left(27\left(\delta-\delta_0\right)k_h^2 - 2k_c^2 + 3\sqrt{3}\sqrt{\left(\delta-\delta_0\right)\left(27\left(\delta-\delta_0\right)k_h^2 - 4k_c^2\right)}k_h \right) \right)^{\frac{1}{3}} \tag{23}$$

When dealing with the friction between disc and casing, the Coulomb model is applied.

$$F_T = \mu F_N \tag{24}$$

In the above expression, μ denotes the Coulomb friction coefficient that is mainly determined by the coatings material.

Based on Eqs. (20) and (21), the impact force and friction force can be divided into two components in the two directions of $o-z$ and $o-y$, namely

$$\begin{cases} F_z\left(z_1, z_2, y_1, y_2\right) = \dfrac{F_T\left(y_1-y_2\right) - F_N\left(z_1-z_2\right)}{\sqrt{\left(z_1-z_2\right)^2 + \left(y_1-y_2\right)^2}} \\ F_y\left(z_1, z_2, y_1, y_2\right) = -\dfrac{F_N\left(y_1-y_2\right) + F_T\left(z_1-z_2\right)}{\sqrt{\left(z_1-z_2\right)^2 + \left(y_1-y_2\right)^2}} \end{cases} \tag{25}$$

Particularly, the energy loss caused by the contact damping is not taken into consideration.

2.3 Dynamic modeling of rotor-casing system subjected to axial load and radial rub

Under the action of unbalanced force of disc, rub-impact force and axial load, the vibration equations of the rotor-casing system can be derived based on the Newton's second law.

$$\begin{cases} m_1\ddot{z}_1 + c_{eq}\dot{z}_1 + k_{eq}z_1 + \alpha z_1\left(z_1^2+y_1^2\right) - F_z\left(z_1, z_2, y_1, y_2\right) = m_1 e\omega^2\cos\left(\omega t\right) \\ m_2\ddot{z}_2 + c_s\dot{z}_2 + k_s z_2 + F_z\left(z_1, z_2, y_1, y_2\right) = 0 \\ m_1\ddot{y}_1 + c_{eq}\dot{y}_1 + k_{eq}y_1 + \alpha y_1\left(z_1^2+y_1^2\right) - F_y\left(z_1, z_2, y_1, y_2\right) = m_1 e\omega^2\sin\left(\omega t\right) \\ m_2\ddot{y}_2 + c_s\dot{y}_2 + k_s y_2 + F_y\left(z_1, z_2, y_1, y_2\right) = 0 \end{cases} \tag{26}$$

where m_1 and m_2 denote the disc mass and casing mass, e denotes the disc eccentricity, ω denotes the rotational speed, c_s denotes the support damping of casing, and k_s denotes the support stiffness of casing, respectively.

2.4 Validity discussion of rotor-casing model

In this section, the validity of the equivalent dynamic model shown in Fig. 3 is examined by

using ANSYS simulation. According to the structural design of the actual rotor test rig and some relevant references [36,37], the structural parameters of the rotor-casing system are listed in Table 1. Meanwhile, the majority of thermal barrier coatings is ZrO_2 (zirconia) stabilized with 7-8 wt% Y_2O_3 (yttria). As introduced in the references [38,39], the elastic modulus of coatings is about 210 GPa at room-temperature. With the sharp increase of environment temperature, the coatings soften significantly. For example, at 1600 ℃, the elastic modulus of coatings will decrease to 10 GPa. Even more serious is that the elastic modulus of coatings may further decrease to about 1 GPa at higher environment temperature.

When dealing with the problem that the hinged-hinged rotating Euler-Bernoulli beam is subjected to axial load, the static buckling load has been derived in [6], so that

$$P_0 = \frac{9.870EI}{l^2} \tag{27}$$

To ensure that the buckling phenomenon of shaft does not happen, the axial load acted on the shaft is set to $N=0.5P_0$.

Table 1 Parameters of the nonlinear rotor-casing system with surface coatings

Physical parameter	Value
Mass of disc m_1 (kg)	58.3613
Mass of casing m_2 (kg)	11.6723
Eccentricity of disc e (mm)	2.2
Radius of disc and casing R_1, R_2 (m)	0.3, 0.3025
Length of shaft l (mm)	448.8
Radius of shaft r (mm)	12.2
Elastic modulus of shaft E (GPa)	210
Equivalent damping of shaft c_{eq} (N.s/m)	261.8
Structural stiffness of casing k_c (MN/m)	3
Support stiffness k_s (MN/m)	20
Support damping c_s (N.s/m)	2100
Elastic modulus of coatings on disc and casing E_1, E_2 (GPa)	210
Poisson ratio of coatings on disc and casing ν_1, ν_2	0.3
Initial clearance between disc and casing δ_0 (mm)	2.5
Frictional coefficient μ	0.1

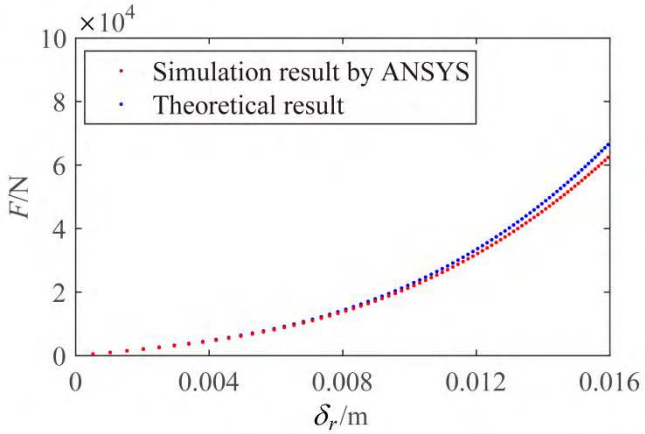

Fig. 6. Comparison between theoretical results and simulation results in the condition of $N=0.5P_0$.

As shown in Fig. 6, the relation between radial displacement of disc and restoring force of shaft F can be obtained by theoretical analysis (Eq. 18) and ANSYS simulation, respectively. It is evident that two methods are match very well in the condition of smaller displacement. With the increase of displacement, the relative error turns to be obvious. However, when the displacement is $\delta_r = 0.016$ m, the maximum error is 7.07%, which also belongs to the permissible range of actual engineering.

From the above analysis, the equivalent dynamic model shown in Fig. 3 is proved to be valid. And then the dynamic characteristics of the model are further analyzed in the next part.

3. General results and discussion

To comprehensively master the operation quality of rotor-casing system, the dynamic characteristics of the system are numerically investigated at different rotational speeds. During the numerical integration, predicting the instantaneous contact is crucial. Therefore, a linear interpolation method is used to modify the time step at some special moments.

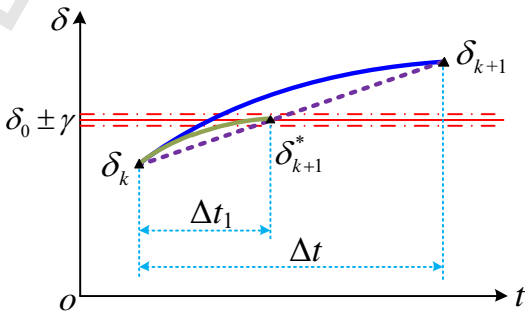

Fig. 7. Schematic diagram of linear interpolation method.

Fig. 7 illustrates the detailed modification of time step, where δ_k and δ_{k+1} respectively

denote the radial relative displacement of disc-casing at the previous moment and the next moment, Δt denotes the time step, γ denotes the calculation tolerance.

In the case of 'no rub-impact to rub-impact', δ_k and δ_{k+1} are supposed to satisfy

$$\begin{cases} \delta_k - \delta_0 \le 0 \\ \delta_{k+1} - \delta_0 > 0 \end{cases} \tag{28}$$

If the condition $\left|\delta_{k+1} - \delta_0\right| \le \gamma$ is achieved, the time remains Δt. Otherwise, the time step is reset by the linear interpolation method, namely

$$\Delta t_1 = \frac{\delta_0 - \delta_k}{\delta_{k+1} - \delta_k} \Delta t \tag{29}$$

By using the above expression Δt_1, the new radial relative displacement δ_{k+1}^* can be recalculated. If the new condition $\left|\delta_{k+1}^* - \delta_0\right| \le \gamma$ is achieved, the modified process is accomplished. Otherwise, the iteration is required to go on.

3.1 Effect of axial load

It can be observed from Eq. (16) that both equivalent linear stiffness and equivalent nonlinear stiffness are affected by the axial load N. Let us define the axial load as $N=\beta P_0$. Then the change rules of them are further given, when the coefficient β is set to $[0, 0.5]$, as shown in Fig. 8. With the increase of the coefficient β, the equivalent linear stiffness k_{eq} gradually decreases. On the contrary, the equivalent nonlinear stiffness α gradually increases.

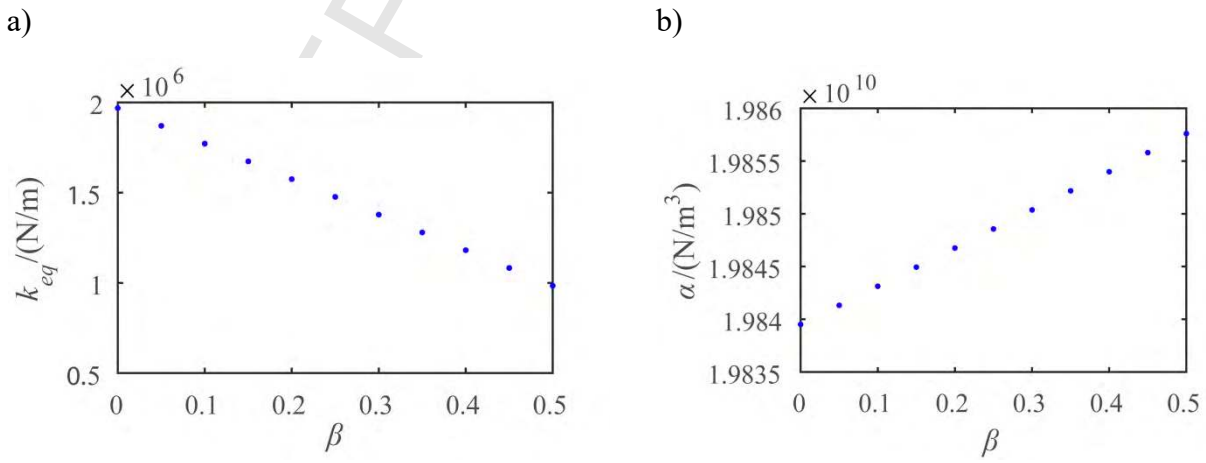

Fig. 8. Effects of axial load on the elastic shaft: (a) equivalent linear stiffness and (b) equivalent nonlinear stiffness.

For complicated rotating machine, it is essential step for engineers to study the vibration of the rotor-casing system with coupling fault in advance. In this section, the nonlinear dynamic responses of the system are analyzed by bifurcation diagram, whirl orbit and waveform.

The bifurcation diagrams of the system without and with axial load are respectively shown in Fig. 9(a) and 9(b), where the horizontal axis represents the rotational speed ω and the vertical axis represents the vertical displacement of disc y_1. At the interval of $100-900$ rad/s, there are rich nonlinear dynamic phenomena, including period, double periods, quasi period and chaos.

By comparing Fig. 9(a) with Fig. 9(b), it can be seen that the response difference caused by the axial load mainly concentrates in the region of lower rotational speed, especially in the range $[100, 200]$ rad/s. To further reveal the detailed difference, the local refined bifurcation diagram is shown in Fig. 10.

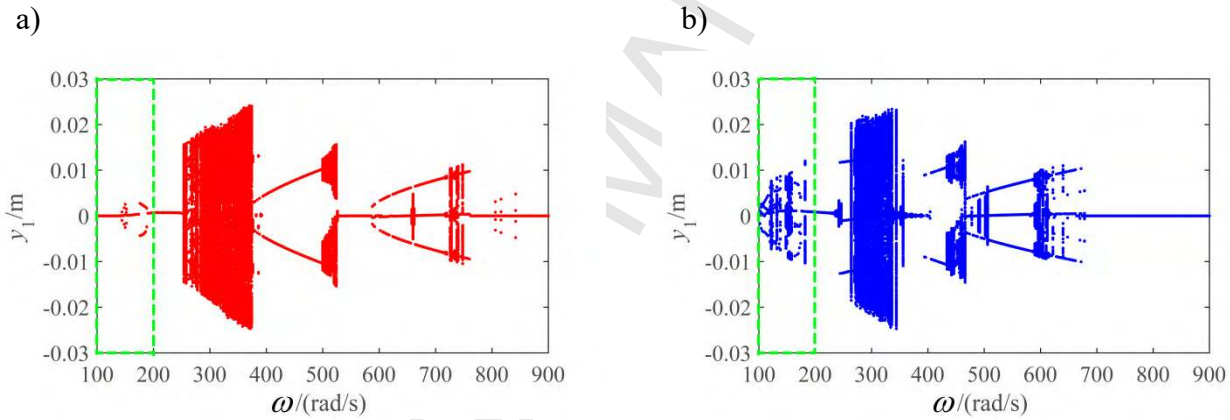

Fig. 9. Bifurcation diagram of the rotor system: (a) without axial load and (b) with axial load $N=0.5P_0$.

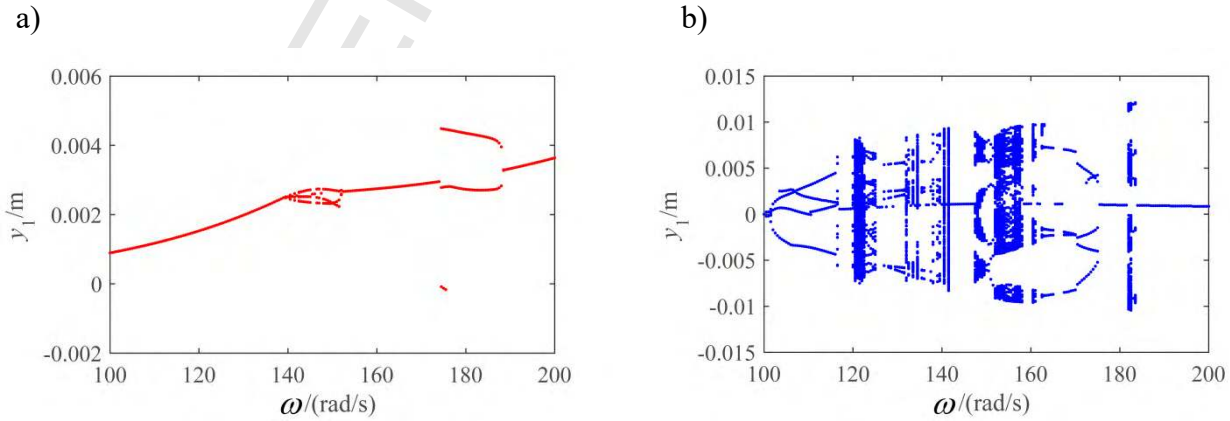

Fig. 10. Local refined bifurcation diagram of the rotor system in the range $[100, 200]$ rad/s: (a)

without axial load and (b) with axial load $N=0.5P_0$.

In the range $[100, 200]$ rad/s, the vibration responses of the system without axial load are mainly identified as periodic motion, such as period-1, period-2 and period-3. However, in the same range of rotational speed, quasi-periodic and chaotic motions happen in that of the system. These phenomena suggest that the original smooth running of the rotor system can be seriously affected by the axial load at the lower rotational speed.

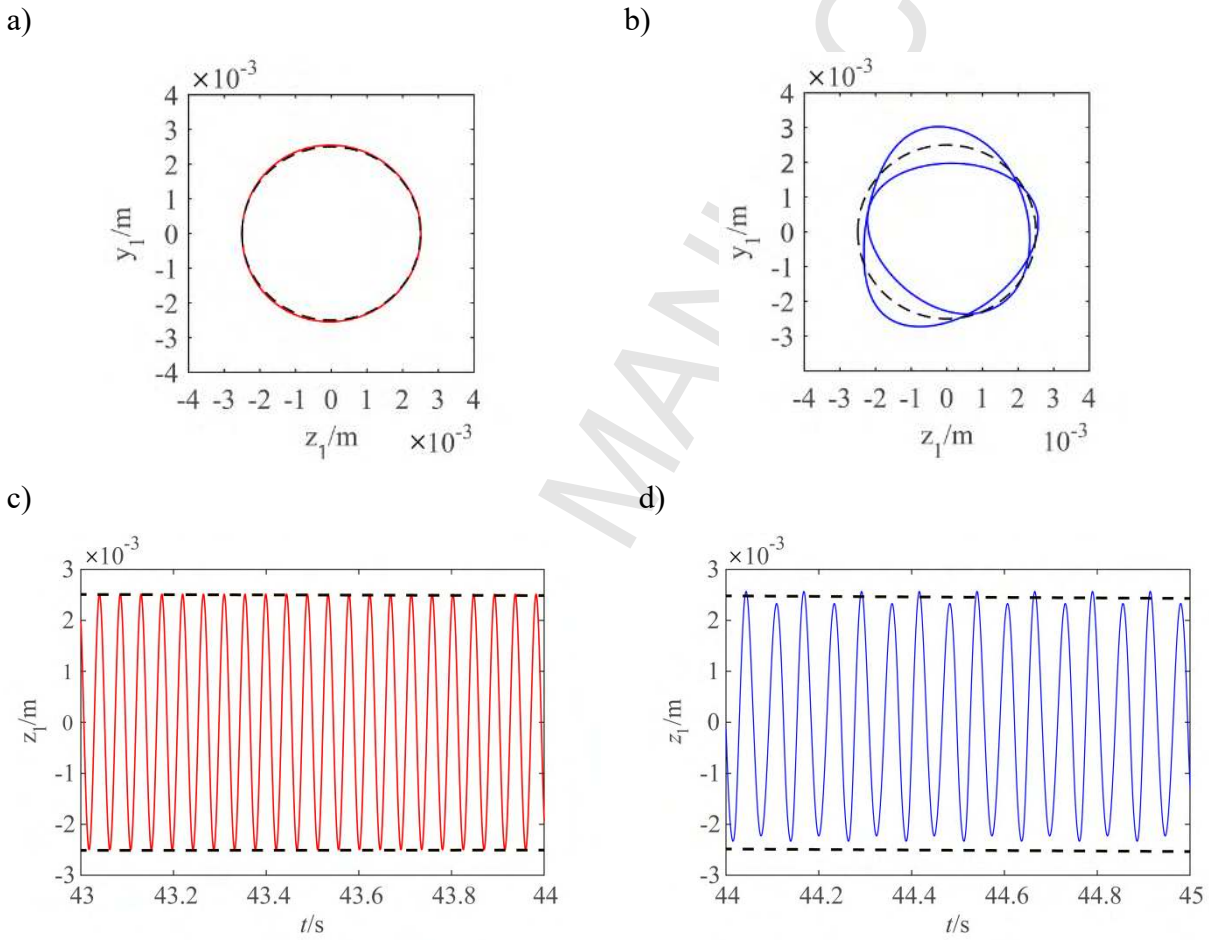

Fig. 11. Vibration response corresponding to the first rub-impact: (a) whirl orbit without axial load, (b) whirl orbit with axial load, (c) waveform without axial load and (d) waveform with axial load.

Additionally, the effects of the axial load N on the rub-impact form and the rotational speed corresponding to the first rub-impact are further investigated. When the shaft is not subjected to the axial load, the rotational speed corresponding to the first rub-impact is about 140 rad/s. Meanwhile, the whirl orbit and waveform shown in Fig. 11(a) and 11(c) indicates that the fault form of the first rub-impact is full annular rubbing. Specifically, the black dotted line represents the initial clearance of disc-casing.

When the shaft is subjected to the axial load, the rotational speed corresponding to the first rub-impact decreases from 140 rad/s to 101 rad/s. And the fault form of the first rub-impact is changed to partial rubbing, as shown in Fig. 11(b) and (d).

Thus, it is concluded that there is a close relationship between axial load and radial rub. The severity of rub-impact can be usually intensified by the axial load at the lower rotational speed.

3.2 Coupling effect of coating hardness and axial load

Compared with the single-parameter analysis of coating hardness [28], the main highlights of this part mainly focus on the coupling effects of coating hardness and axial load. The contents of coupling effects mean that when the axial load acts on the shaft, the dynamics variation rules caused by coating hardness are revealed at the lower rotational speed, which is less than the first critical speed.

Considering the effects of the higher environment temperature, the severe coating softening happens. Therefore, keeping the other parameters illustrated in Table 1 constant, the coating hardness is reset to 10 GPa and 1 GPa, respectively.

In the condition of 10 GPa, the bifurcation diagram of the system subjected to axial load is numerically calculated. By comparing Fig. 9(b) with Fig. 12(a), it can be seen that the dynamic behaviors at the interval of lower rotational speed are obviously affected by the coating hardness. When the rotational speed is less than the first critical speed, the rotational speed range of quasi-period and chaos becomes relatively narrower. However, with the increase of rotational speed, the response differences between Fig. 9(b) and Fig. 12(a) are not obvious.

As shown in Fig. 12(b), the original complicated dynamic phenomena of the system at the interval of lower rotational speed are replaced by the periodic motions, such as period-1, period-2 and period-3. These phenomena suggest that when the rotor system is under combined action of axial load and radial rub, the influences of coating hardness mainly focus on the vibration characteristics of the system in the range of lower rotational speed.

When the rotational speed is ω=148 rad/s, the whirl orbits of the rotor system with different coating hardness are shown in Fig. 13. In the conditions of 210 GPa and 10 GPa, a lot of irregular curves occurs in the whirl orbit of the system, as shown in Fig. 13(a) and 13(b). When the coating hardness decreases to 1 GPa, the vibration amplitude becomes smaller and the whirl orbit is shown in the form of a single loop (see Fig. 13(c)). Additionally, the variation rules of whirl orbit also

suggest that the rub-impact form gradually varies from partial rub-impact to full annular rubbing with the decrease of coating hardness.

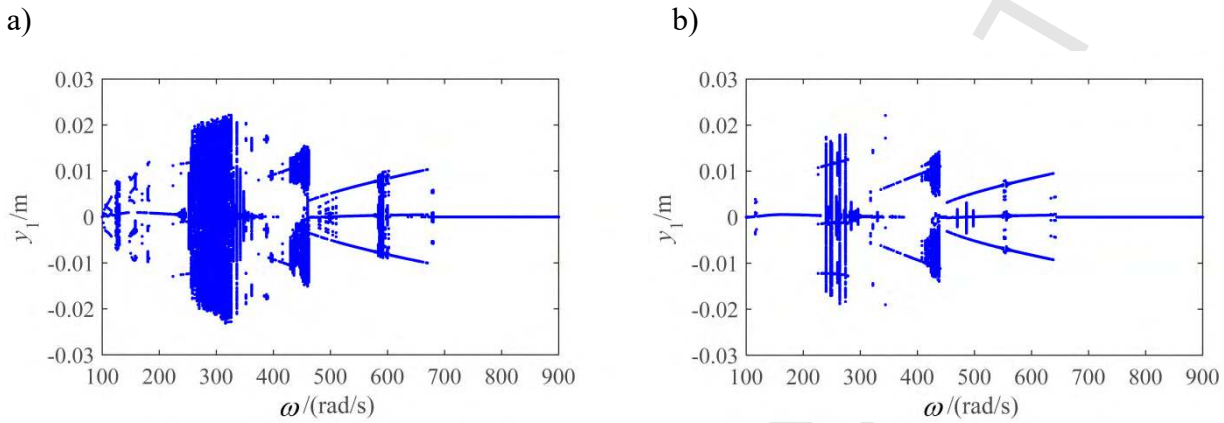

Fig. 12. Coupling effects of axial load and radial rub on the bifurcation diagram of the rotor system: (a) E_1=E_2=10 GPa and (b) E_1=E_2=1 GPa.

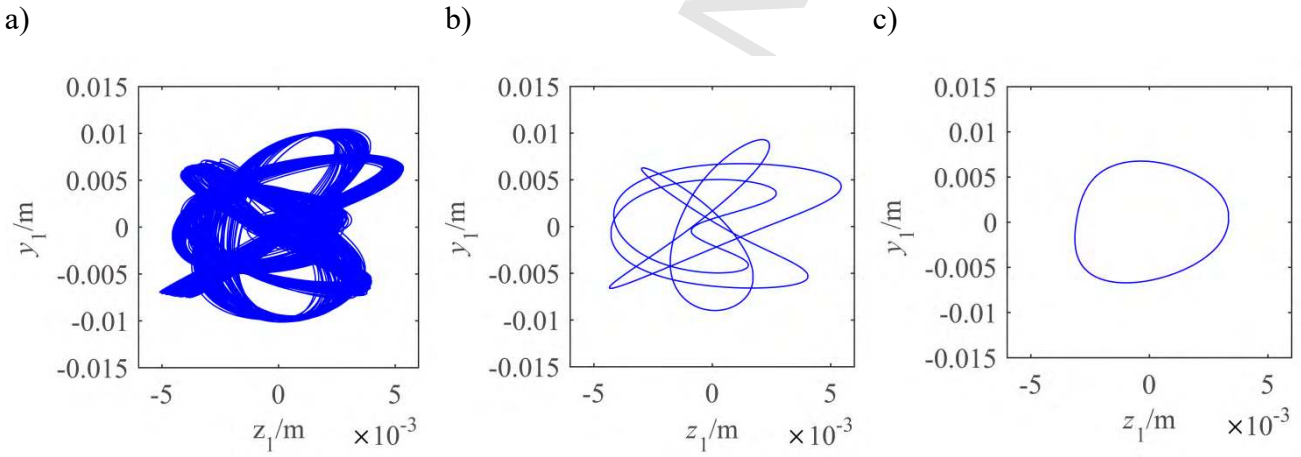

Fig. 13. At ω=148 rad/s, the variations of whirl orbit of the rotor system with different coating hardness: (a) E_1=E_2=210 GPa, (b) E_1=E_2=10 GPa and (c) E_1=E_2=1 GPa.

3.3 Effect of support stiffness of casing

As for the rotor-casing system shown in Fig. 1, the support stiffness of casing is a key parameter, which reveals the constraint degree of casing and directly affects the relative displacement of disc-casing. Therefore, the bifurcation diagram of the rotor system with different support stiffness of casing is analyzed in this section, where the stiffness is reset to $k_s = 2$ MN/m and $k_s = 200$ MN/m, respectively.

As shown in Fig. 14(a), the system responses are exhibited as the alternate forms of periodic motion, quasi-periodic motion and chaos at the interval of $100-800$ rad/s. From then, the rotor

system enters into the irregular motion and remains the state up to $900\ \mathrm{rad/s}$. Overall, the rotational speed range of periodic motion is wider than that of quasi-periodic and chaotic motion.

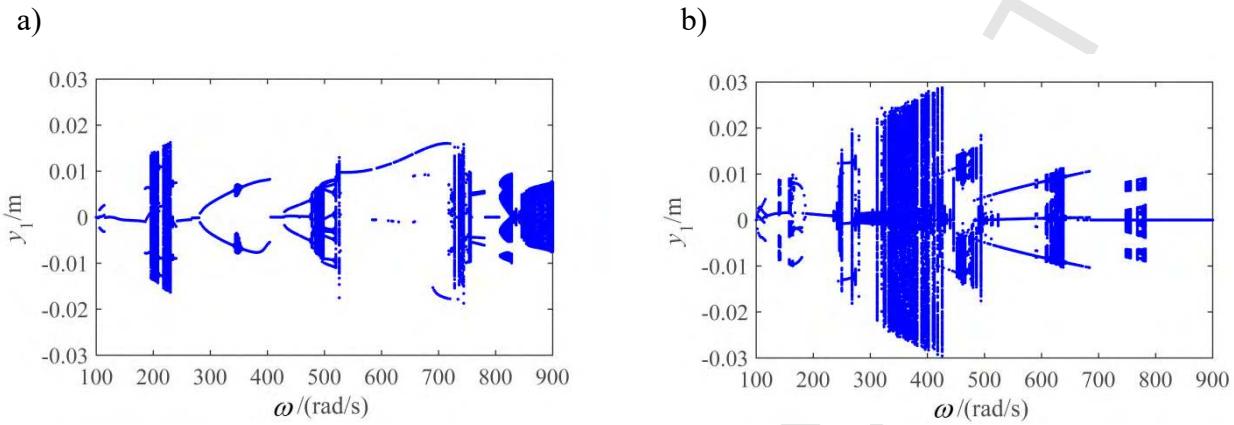

Fig. 14. Bifurcation diagram of the rotor system with different support stiffness of casing: (a) $k_s = 2$ MN/m and (b) $k_s = 200$ MN/m.

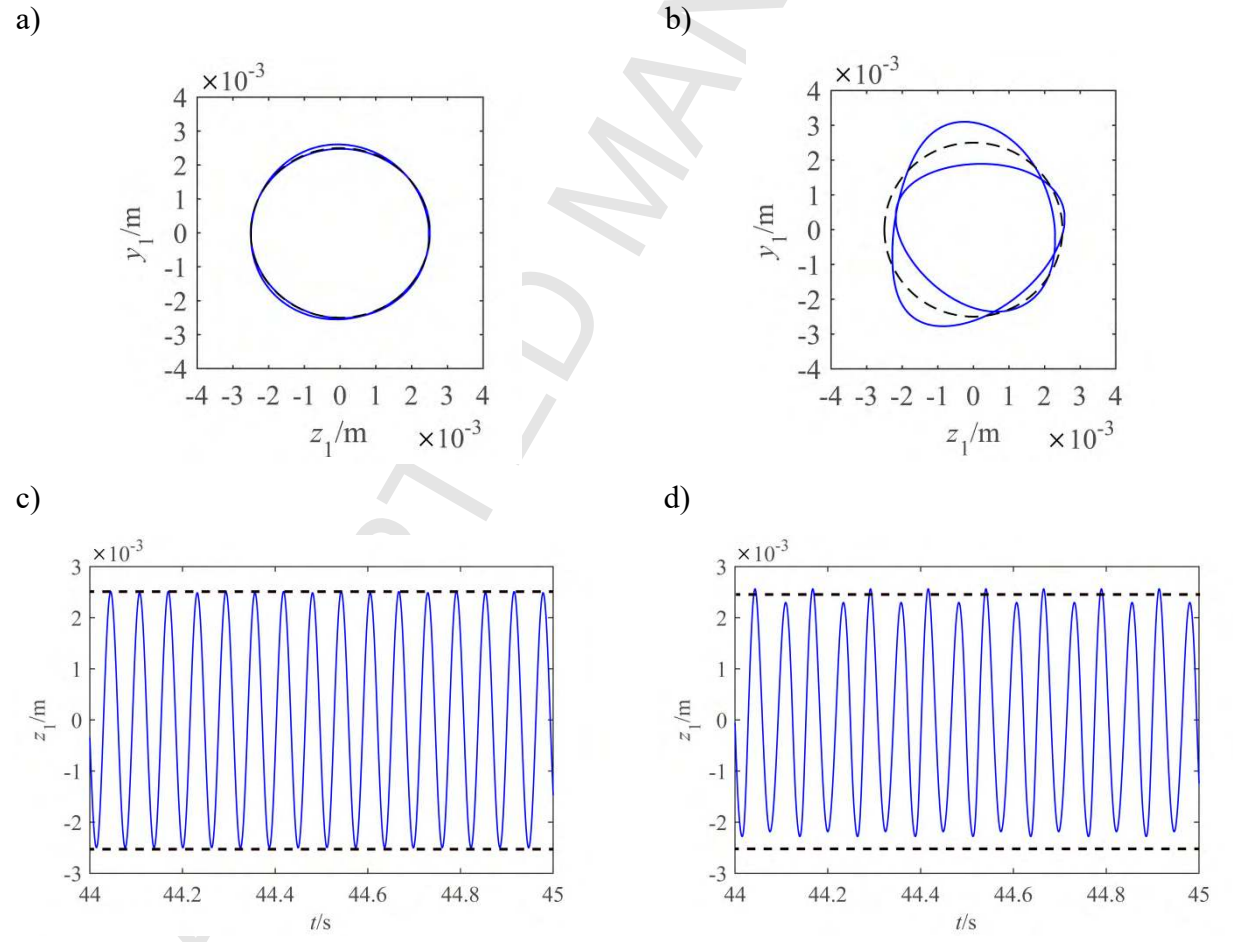

Fig. 15. Vibration responses corresponding to the first rub-impact in the different conditions of support stiffness of casing: (a) whirl orbit in the condition of $k_s = 2$ MN/m, (b) whirl orbit in the

condition of $k_s = 200$ MN/m, (c) waveform in the condition of $k_s = 2$ MN/m and (d) waveform in the condition of $k_s = 200$ MN/m.

When the support stiffness of casing is set to $k_s = 200$ MN/m, the bifurcation diagram of the rotor system is given in Fig. 14(b). It is clear that in the range $100-800$ rad/s, the vibration responses of the system become more complicated and the rotational speed range corresponding to irregular motion tends to be wider. With the further increase of rotational speed, the irregular motion is replaced by the 1*T*-periodic motion. Therefore, it can be concluded that there is a close relation between dynamic characteristics of the rotor system and support stiffness of casing.

Moreover, the effects of support stiffness of casing on the first rub-impact between disc and casing are investigated, including the rotational speed corresponding to the first rub-impact and the fault form of the first rub-impact. For the case of $k_s = 2$ MN/m, the rotational speed corresponding to the first rub-impact is about ω=101 rad/s and the fault form is identified as slight partial rubbing, as shown in Fig. 15(a) and 15(c). If the support stiffness of casing is modified as $k_s = 200$ MN/m, the rotational speed corresponding to the first rub-impact remains unchanged. However, the penetration between casing and disc becomes serious, as shown in Fig. 15(b) and 15(d). Thus, reducing support stiffness of casing may be an effective method to alleviate the rub-impact between disc and casing.

4. Conclusion

Taking a rotor-casing system subjected to axial load and radial rub as the research object, the corresponding dynamic model has been established in this paper. Due to the unbalanced excitation of disc, the rub-impact of disc-casing with coatings has happened and then the mechanical mechanism of rub-impact has been described by the different contact model during the different penetration process. Meanwhile, the Coulomb model has been applied to simulate the friction characteristics. Then the nonlinear dynamic behaviors of the rotor system with coupling fault have been analyzed by bifurcation diagram. Moreover, both whirl orbit and waveform have been used to identify the rub-impact form, such as full annular rubbing and partial rubbing. Finally, the effects of axial load, coating hardness and support stiffness of casing have been discussed respectively. Some conclusions drawn from the study can be summarized as follows:

(1) For the geometric nonlinear shaft, axial load can decrease the equivalent linear stiffness of shaft while it can increase the equivalent nonlinear stiffness of shaft.

(2) Axial load acting on the shaft more easily leads to the occurrence of complicated nonlinear dynamic phenomena, especially in the range of lower rotational speed.

(3) Due to the effects of axial load, the protection of motion stability given by coatings mainly concentrates on the range of lower rotational speed, which is usually less than the first critical speed.

(4) To some extent, decreasing the support stiffness of casing can relieve rub-impact harm and further guarantee well operation of rotating machine.

Acknowledgment

This work was supported by the National Nature Science Foundation of China (Grant No. 11702228), (Grant No. 11372258) and the Fundamental Research Funds for the Central Universities (2682017CX087).

References

[1] M. Chamoun, R. Rulliere, P. Haberschill, et al., Modelica-based modeling and simulation of a twin screw compressor for heat pump applications, Appl. Therm. Eng. 58(1-2) (2013) 479-489.

[2] Y. He, F. Cao, L. Jin, et al., Experimental study on the performance of a vapor injection high temperature heat pump, Int. J. Refrigeration. 60 (2015) 1-8.

[3] X. Wu, Z. Xing, Z. He, et al., Performance evaluation of a capacity-regulated high temperature heat pump for waste heat recovery in dyeing industry, Appl. Therm. Eng. 93 (2016) 1193-1201.

[4] C. Bai, H. Zhang, Almost sure asymptotic stability of rotor systems subjected to stochastical axial loads, Mech. Mach. Theory. 58 (2012) 192-201.

[5] H.D. Nelson, A finite rotating shaft element using Timoshenko beam theory, J. Mech. Des. 102 (1980) 793-803.

[6] L.W. Chen, D.M. Ku, Dynamic stability analysis of a rotating shaft by the finite element method, J. Sound Vib. 143 (1990) 143-151.

[7] X.L. Leng, G. Meng, T. Zhang, et al., Bifurcation and chaos response of a cracked rotor with random disturbance, J. Sound Vib. 299 (2007) 621-632.

[8] C.P. Chen, Y.M. Fu, Nonlinear dynamic stability for elastic shaft-disc rotating system under the periodic axial load, J. Hunan Univ. 30(3) (2003) 19-23. (in Chinese)

[9] H. Ma, Q. Zhao, X. Zhao, et al., Dynamic characteristics analysis of a rotor-stator system under different rubbing forms, Appl. Math. Model. 39 (2015) 2392-2408.

[10] L. Xiang, A.J. Hu, L.L. Hou, et al., Nonlinear coupled dynamics of an asymmetric double-disc rotor-bearing system under rub-impact and oil-film forces, Appl. Math. Model. 40 (2016) 4505-4523.

[11] Y.X. Wang, R. Markert, J.W. Xiang, et al., Research on variational mode decomposition and its application in detecting rub-impact fault of the rotor system, Mech. Syst. Signal Process. 60-61 (2015) 243-251.

[12] C.W. Chang-Jiang, C.K. Chen, Chaos of rub-impact rotor supported by bearings with nonlinear suspension, Tribol. Int. 42 (2009) 426-439.

[13] H.M. Khanlo, M. Ghayour, S. Ziaei-Rad, Chaotic vibration analysis of rotating, flexible, continuous shaft-disk system with a rub-impact between the disk and the stator, Commun. Nonlinear Sci. Numer. Simul. 16 (2011) 566-582.

[14] J. Jiang, H. Ulbrich, Stability analysis of sliding whirl in a nonlinear Jeffcott rotor with cross coupling stiffness coefficients, Nonlin. Dyn. 24(3) (2001) 269-283.

[15] J. Yu, On occurrence of reverse full annular rub. J. Eng. Gas Turbine Power. 134 (2012) 219-227.

[16] F. Chu, Z. Zhang, Bifurcation and chaos in a rub-impact Jeffcott rotor system, J. Sound Vib. 210(1) (1998) 1-18.

[17] N. Vlajic, X. Liu, H. Karki, B. Balachandran, Torsional oscillations of a rotor with continuous stator contact, Int. J. Mech. Sci. 83 (2014) 65-75.

[18] N. Vlajic, C.M. Liao, H. Karki, B. Balachandran, Draft: stick-slip motions of a rotor-stator system, J. Vib. Acoust. 136(2) (2014) 021005-1-021005-8.

[19] T.H. Patel, A.K. Darpe, Vibration response of a cracked rotor in presence of rotor-stator rub. J. Sound Vib, 317 (2008) 841-865.

[20] Z. Huang, J. Zhou, M. Yang, et al., Vibration characteristics of a hydraulic generator unit rotor system with parallel misalignment and rub-impact, Arch. Appl. Mech. 81(7) (2011) 829-838.

[21] L. Xiang, A. Hu, L. Hou, et al., Nonlinear coupled dynamics of asymmetric double-disc rotor-bearing system under rub-impact and oil-film forces, Appl. Math. Model. 40(7-8) (2015) 4505-4523.

[22] Y. Yang, D.Q. Cao, D.Y. Wang, Investigation of dynamic characteristics of a rotor system with

surface coatings, Mech. Syst. Signal Process. 84 (2017) 469-484.

[23] D.Q. Cao, Y. Yang, H.T. Chen, et al., A novel contact force model for the impact analysis of structures with coating and its experimental verification, Mech. Syst. Signal Process. 70-71 (2016) 1056-1072.

[24] T.N. Rhys-Jones, Thermally sprayed coating systems for surface protection and clearance control applications in aero engines, Surf. Coat. Technol. 43-44 (1990) 402-415.

[25] B. Gleeson, Thermal barrier coatings for aeroengine applications, J. Propuls. Power. 22(2) (2006) 375-383.

[26] M. Yi, J. He, B. Huang, et al., Friction and wear behavior and abradability of abradable seal coating, Wear. 231(1) (1999) 47-53.

[27] A. Batailly, M. Legrand, A. Millecamps, et al., Numerical-experimental comparison in the simulation of rotor/stator interaction through blade-tip/abradable coating contact, J. Eng. Gas. Turbines Power-Trans. ASME. 134(8) (2012) 082504.

[28] Y. Yang, D.Q. Cao, Y.Q. Xu, Rubbing analysis of a nonlinear rotor system with surface coatings, Int. J. Nonlinear Mech. 84 (2016) 105-115.

[29] J.P. Den Hartog, Forced vibrations with combined coulomb and viscous friction, Trans. ASME APM. 53-9 (1931) 107-115.

[30] H.M. Khanlo, M. Ghayour, S. Ziaei-Rad, The effects of lateral-torsional coupling on the nonlinear dynamic behavior of a rotating continuous flexible shaft-disk system with rub-impact, Commun Nonlinear Sci. Numer. Simul. 18 (2013) 1524-1538.

[31] W.M. Zhang, G. Meng, D. Chen, et al., Nonlinear dynamics of a rub-impact micro-rotor system with scale-dependent friction model, J. Sound Vib. 309 (2008) 756-777.

[32] S. Lahriri, H.I. Weber, I.F. Santos, et al., Rotor-stator contact dynamics using a non-ideal drive—Theoretical and experimental aspects, J. Sound Vib. 331 (2012) 4518-4536.

[33] C.A.L.L. Fonseca, R.R. Aguiar, H.I. Weber, On the non-linear behavior and orbit patterns of rotor/stator contact with a non-conventional containment bearing, Int. J. Mech. Sci. 105 (2016) 117-125.

[34] P. Varney, I. Green, Nonlinear phenomena, bifurcations, and routes to chaos in an asymmetrically supported rotor-stator contact system, J. Sound Vib. 336 (2015) 207-226.

[35] T.H. Patel, A.K. Darpe, Coupled bending-torsional vibration analysis of rotor with rub and crack,

J. Sound Vib. 326 (2009) 740-752.

[36] H.B. Zhang, Y.S. Chen, J. Li, Bifurcation on synchronous full annular rub of rigid-rotor elastic-support system, Appl. Math. Mech. –Engl. Ed. 33(7) (2012) 865-880.

[37] X.L. Zhang, J. Jiang, Global dynamical characteristics of rotor/stator systems accounting for stator mass and contact surface stiffness, Chin. J. Appl. Mech. 24(3) (2007) 380-385 (in Chinese).

[38] Y. Tian, C. Chen, J. Liu, et al., Research and development of ZrO2 thermal barrier coatings, Chin. Mech. Eng. 16(16) (2005) 1499-1503.

[39] C. Batista, A. Portinha, R.M. Ribeiro, et al., Surface laser-glazing of plasma-sprayed thermal barrier coatings, Appl. Surf. Sci. 247 (2005) 313-319.

Highlights

1. A complicated dynamic model for rotor-casing system subjected to axial load and radial rub is established and verified.

2. Nonlinear dynamic characteristics of the fault system at different rotational speeds are analyzed.

3. Effects of axial load, casing support and coating hardness on the vibration response and rub-impact form are discussed.